Available online at www.sciencedirect.com
SCIENCE DIRECT®
Optical Materials 28 (2006) 935–943
OPTICAL Materials
www.elsevier.com/locate/optmat

Crystallization, texture and second-harmonic generation in TiO_2–BaO–B_2O_3 glasses

C.A.C. Feitosa [a,b], V.R. Mastelaro [b,*], A.R. Zanatta [b], A.C. Hernandes [b], E.D. Zanotto [c]

[a] Universidade Federal do Maranhão, São Luís, MA, Brazil
[b] Instituto de Física de São Carlos, Universidade de São Paulo, Caixa Postal 369, 13560-970, São Carlos, SP, Brazil
[c] Laboratório de Materiais Vítreos, Departamento de Engenharia de Materiais, Universidade Federal de São Carlos, São Carlos, SP, Brazil

Received 13 October 2004; accepted 5 May 2005
Available online 5 July 2005

Abstract

Partially crystallized glasses containing non-centrosymmetric β-BaB_2O_4 (β-BBO) and/or $BaTi(BO_3)_2$ crystals were prepared by controlled surface crystallization of x_1TiO_2–x_2BaO–$x_3B_2O_3$ glasses, where $x_1 = 4\%$, 8%, 15% and $x_2/x_3 = 8/9$ (mol%). Differential thermal analyses were made to select appropriate heat treatments to partially crystallize some samples. The resulting crystalline phases were determined by X-ray diffraction and micro-Raman spectroscopy. Spontaneous preferred orientation (texture) occurred on the surface of all these glasses. Samples with $x_1 = 4\%$ and 8% heat-treated from 1 to 32 h showed only β-BaB_2O_4 precipitated on the glass surfaces, while the glass with $x_1 = 15\%$ only had $BaTi(BO_3)_2$ in samples heat-treated for less than 8 h. Longer treatments also led to crystallization of β-BaB_2O_4, occurring preferentially between the arms or underneath the $BaTi(BO_3)_2$ crystals, but present on the glass surface as well, and this became the predominant crystalline phase. Some surface crystallized glasses yielded a reasonable second-harmonic generation. The non-linear optical coefficient, d_{eff}, in the $x_1 = 15\%$ crystallized sample was 1.1 pm/V, which corresponds to approximately 50% of that observed in the β-BBO single crystal.

Keywords: Barium borate; Glass; Surface crystallization; Texture; Second-harmonic generation

1. Introduction

The crystallization pathways and kinetics of ternary TiO_2–BaO–B_2O_3 glasses were first studied due to their potential as ferroelectric glass–ceramics containing $BaTiO_3$ crystals [1–3]. More recently, this glass system has been widely studied because crystallization can lead to the formation of an interesting crystalline phase, β-BaB_2O_4 (herein after denoted as β-BBO) [4–6]. Its physical properties, such as a high effective second-harmonic generation coefficient, wide-range transparency and high damage threshold are suitable for several optical applications [7]. High values of second-harmonic generation (SHG) signals have been observed in some glass–ceramics when a crystalline phase with a high SHG efficiency is precipitated from the glass [8,9].

Surface crystallized glasses containing β-BBO were first obtained by Ding et al. [4] from a $15TiO_2$–$40BaO$–$45B_2O_3$ (mol%) glass. According to those authors, application of an ultrasonic technique for surface modification with an aqueous suspension of β-BBO particles prior to heating enhanced the surface nucleation density of the β-BBO phase, resulting in a dense transparent β-BBO crystallized layer.

The devitrification process of glasses of the $xTiO_2$–$(50 - x/2)BaO$–$(50 - x/2)B_2O_3$ system, with $x = 4$, 8,

* Corresponding author. Tel.: +55 16 3373 9828; fax: +55 16 3373 9824.
E-mail address: valmor@if.usp.sc.br (V.R. Mastelaro).

0925-3467/$ - see front matter © 2005 Elsevier B.V. All rights reserved.
doi:10.1016/j.optmat.2005.05.003

and 16 mol%, was studied by Pernice et al. [5] and Aronne et al. [6]. According to these authors, surface crystallization predominates in all these glasses and, upon devitrifying, they form mainly β-BBO microcrystals. In powder samples containing 8% and 16% of TiO_2, the aforementioned authors also observed the formation of $BaTi(BO_3)_2$ and $Ba_4B_2O_7$.

In recent papers [10,11], some of us described the surface crystallization of a $15TiO_2$–$40BaO$–$45B_2O_3$ glass irradiated by a CO_2 laser beam. We observed the precipitation of $BaTi(BO_3)_2$ in the early stages of crystallization, although the predominant crystalline phase after long periods of thermal treatment was β-BBO [10,11].

Preferential orientation or texture has been extensively studied because most of the technically interesting properties of polycrystalline materials are strongly influenced by texture-related anisotropy. Various methods have been applied to glass–ceramics to obtain defined crystallographic orientation, e.g., solid-state epitaxy [12–14], glass extrusion [15–17] or temperature gradients [18].

It is also known that *spontaneous* preferential growth of certain crystallographic planes may occur in certain situations from the external glass surfaces towards the glass interior, leading to textured microstructures and yielding properties that are peculiar to some oriented glass–ceramics [19,20].

Although crystallization of the β-BBO phase from BaO–B_2O_3–TiO_2 glasses has been described in the literature, to the best of our knowledge, no information has been reported on the existence of *spontaneous orientation* of β-BBO crystals via surface devitrification of BaO–B_2O_3–TiO_2 glasses. Moreover, according to Ding et al. [4], preferred directions of crystal growth for the β-BBO phase were only obtained when the glass surface was subjected to prior ultrasonic treatment with β-BBO particles uniformly dispersed on the glass surface.

In this work, we studied the crystallization kinetics of controlled surface devitrification of x_1TiO_2–x_2BaO–$x_3B_2O_3$ glasses, where $x_1 = 4\%$, 8% and 15% and $x_2/x_3 = 8/9$ (mol%). These compositions were chosen because, according to previous works, the difficulty of obtaining the β-BBO phase from the $50BaO$–$50B_2O_3$ stoichiometric composition was overcome by the addition of TiO_2. Heating such glasses to 620 °C yield β-BBO and/or $BaTi(BO_3)_2$ crystals [4–6]. Moreover, we characterized the coefficient of second-harmonic generation of some surface crystallized samples.

2. Experimental

The glasses were prepared by mixing appropriate amounts of reagent grade $BaCO_3$, TiO_2 and B_2O_3, and melting them in a platinum crucible in an electrically heated furnace for 3 h at 1100 °C. The melt was quenched on a steel plate and annealed in a furnace at 450 °C for 1 h. This process yielded 4-mm thick, 20 g glass plates. Table 1 gives the batch compositions of these mixtures. To obtain surface crystallized specimens, some samples were mechanically polished to a mirror surface and then heat-treated at 620 °C in air in an electrically heated furnace for periods varying from 1 h to 32 h. Glassy and crystallized powders were obtained by crushing small pieces of glass and partially crystallized samples. The powdered samples were then sieved to less than 5 μm. To use as reference compounds, β-BBO and $BaTi(BO_3)_2$ crystals were prepared by mixing appropriate amounts of reagent grade $BaCO_3$, TiO_2 and B_2O_3 and heating. The β-BBO sample crystallized during cooling its melt, while the $BaTi(BO_3)_2$ phase was obtained by crystallizing its glassy phase by heating it at 620 °C during 12 h.

Table 1
Batch compositions of x_1TiO_2–x_2BaO–$x_3B_2O_3$ samples in mole percent

Glass	x_1, x_2 and x_3 (mol%)
4% TiO_2	4%, 45.2% and 50.8%
8% TiO_2	8%, 43.3% and 48.7%
15% TiO_2	15%, 40% and 45%

Differential thermal analyses (DSC-2910—TA Instruments) were made to select appropriate heat treatments. The crystalline phases present in heat-treated samples were investigated by X-ray diffraction (Rigaku Denki powder diffractometer with geometry θ–2θ, rotating anode X-ray source, Cu Kα radiation, $\lambda = 1.542$ Å, and scintillation detector) and micro-Raman spectroscopy (Renishaw R2000system). The glass and partially crystallized samples were excited with a 488 nm Ar line. The Raman spectra were collected between 300 cm^{-1} and 1800 cm^{-1}, with a spectral resolution of about 1 cm^{-1}. The microstructures of surface crystallized samples were investigated by optical (DMLM Leica) and scanning electron microscopy (DSM 960 Zeiss).

The second-harmonic (SH) intensities of the surface crystallized samples were evaluated by a SHG measuring technique [21]. The 1.064 μm output of a Nd:YAG laser (Spectron Laser Systems, Model SL404G), operating at a 30 Hz repetition frequency, was used as the pump beam. The sample was mounted on a rotation stage to enable rotation around the axis normal to its surface (ϕ) and inclined in relation to the beam by rotation about the axis normal to the beam and parallel to its surface (θ), based on the configuration of the Maker fringe technique [22]. The SH intensities of the sample (I_s) and of a Y-cut quartz reference (I_Q) were measured. A Y-cut quartz crystal plate (0.55 mm) was used as a reference to determine the magnitude of the maximum effective second-order optical non-linearity coefficient (d_{eff}) of the surface crystallized glasses. The fundamental incidence and the transmitted SH light beams were p-

polarized. Narrow-band filters and monochromators were placed in front of the detectors to ensure that only the SH ($\lambda = 0.532$ μm) intensities were measured.

3. Results

3.1. Glass crystallization and resulting microstructures

We recorded differential thermal analysis (DTA) curves of powdered samples with grain sizes smaller than 5 μm, in air, at a heating rate of 10 K/min. From these curves we obtained the glass transition temperatures (T_g) and crystallization peak temperatures (T_c) of all the glasses (Fig. 1). The crystalline phases present in powdered samples heat-treated at the crystallization peak maxima were investigated by XRD. Depending on the glass composition, we identified the following phases: BaB_4O_7 (JCPDS card No. 15-0860), $BaTi(BO_3)_2$ (JCPDS card No. 35-0825), and β-BBO (JCPDS card No. 80-1489). The surface fraction of each crystalline phase was estimated based on the intensity of the main diffraction peaks of each crystalline phase. Based on this analysis, it was possible to identify each crystallization peak in the DTA curves shown in Fig. 1. The fraction of each crystalline phase and T_g and T_c values are shown in Tables 2 and 3, respectively.

To obtain surface crystallized samples, all the glasses were heat-treated at 620 °C for different periods of time. This temperature is below the maximum (DTA) crystallization temperature, and higher than T_g for all the glass compositions studied. Samples of the $x_1 = 4\%$ glass were heat-treated for 1, 2, 16 and 32 h; the $x_1 = 8\%$ glass samples were heat-treated for 2, 4, 16 and 32 h, and the $x_1 = 15\%$ glass samples were heat-treated for 4, 8, 16 and 32 h. Fig. 2 and 3 show the XRD patterns of the surface crystallized bulk samples with $x_1 = 4\%$ and 8%, respectively.

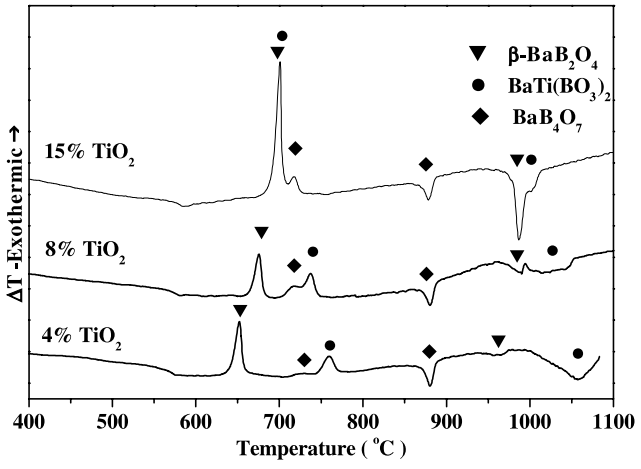

Fig. 1. DTA curves of powdered samples. Experiments in air with a heating rate of 10 K/min, particle size less than 5 μm and sample mass around 30 mg.

Table 2
Fraction of crystalline phases present on the surface of heat-treated powdered samples

Glass	β-BaB_2O_4	$BaTi(BO_3)_2$	BaB_4O_7
4% TiO_2	84%	12%	4%
8% TiO_2	74%	23%	3%
15% TiO_2	47%	49%,	4%

The two samples displayed similar X-ray patterns as the period of treatment increased. After 1 h of heat treatment, the $x_1 = 4\%$ sample showed five diffraction peaks, while the first diffraction peaks of the $x_1 = 8\%$ sample only appeared after 2 h of heat treatment. All the diffraction peaks of the four patterns of each sample were ascribed to the β-BBO phase (JCPDS card No. 80-1489). For the $x_1 = 4\%$ sample, the (1 0 4) diffraction peak was the most intense, regardless of the heat treatment time. For the $x_1 = 8\%$ sample, the (0 0 6) diffraction peak was the most intense after 4 h of heat treatment. The (1 0 4) diffraction peak became the most intense one for the $x_1 = 8\%$ sample heat-treated for a long period of time.

The most intense peaks of the powder diffraction pattern of β-BBO phase were related to the (1 1 3) and (3 0 0) planes, while the most intense peaks in bulk the $x_1 = 4\%$ and $x_1 = 8\%$ samples were those related to the (1 0 4) and (0 0 6) planes, indicating the existence of preferred orientation in these directions. However, the preferred orientation in the (0 0 6) direction in the $x_1 = 8\%$ sample disappeared after prolonged heating.

Fig. 4 presents the X-ray diffraction patterns of the surface crystallized $x_1 = 15\%$ sample. First, diffraction peaks were only observed after 4 h of treatment at $T = 620$ °C, confirming that TiO_2 improves the glass stability towards devitrification. Moreover, a sample heat-treated for 8 h showed only three diffraction peaks. Only when the sample was heat-treated for 16 and 32 h the presence of other diffraction peaks and a significant change in the intensity of the peaks were detected. According to Ding et al. [4], the $15TiO_2$–$40BaO$–$45B_2O_3$ glass they crystallized at different temperatures and time periods contained only the β-BBO phase. In contrast, Pernice et al. [5] and Aronne et al. [6] identified β-BBO and $BaTi(BO_2)_3$ after non-isothermal heating of a $16TiO_2$–$42BaO$–$42B_2O_3$ glass powder. Any attempt to separate the contribution of these two crystalline phases from X-ray diffraction experiments has been unfruitful because several diffraction peaks in their X-ray patterns are coincident. Thus, the attribution of the X-ray diffraction peaks presented on Fig. 4, is based on the order of appearance of crystal phases proved by micro-Raman studies discussed later.

Table 3
Glass transition and crystallization peak temperatures for polycrystalline powders

Sample	T_g (°C)	T_c[a] (°C)	T_c[b] (°C)	T_c[c] (°C)	T_f[a] (°C)	T_f[b] (°C)	T_f[c] (°C)
4% TiO_2	556	652	730	759	880	961	1057
8% TiO_2	567	675	717	737	880	980	1020
15% TiO_2	580	700	717	700	878	986	1000

[a] β-BaB_2O_4.
[b] $BaTi(BO_3)_2$.
[c] BaB_4O_7.

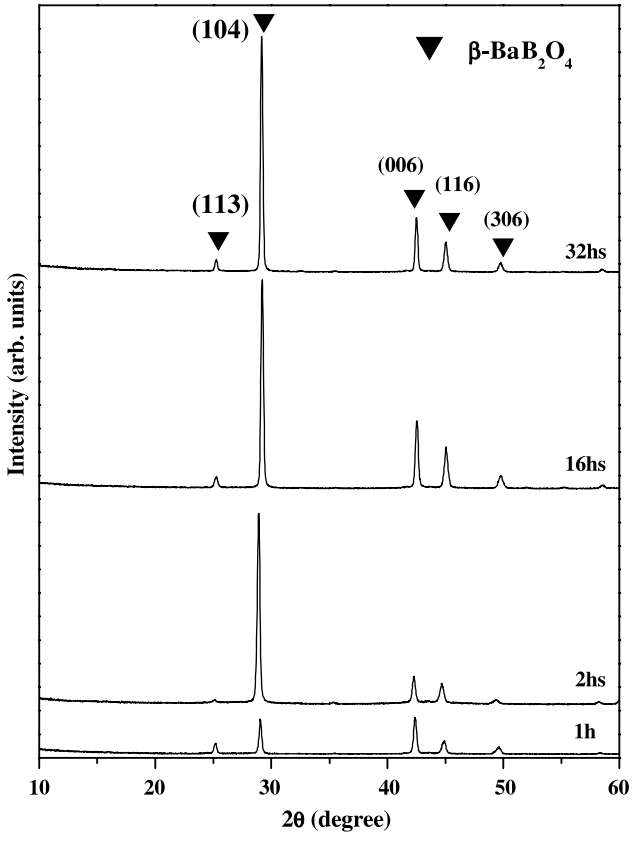

Fig. 2. XRD patterns of a surface crystallized bulk sample with $x_1 = 4\%$, heat-treated for periods varying from 2 to 32 h.

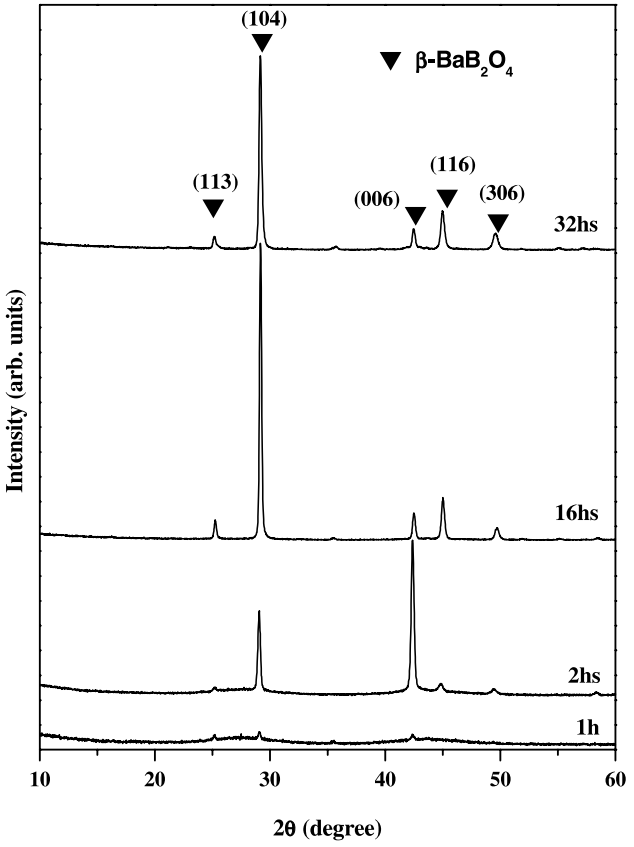

Fig. 3. XRD patterns of a surface crystallized bulk sample with $x_1 = 8\%$, heat-treated for periods varying from 2 to 32 h.

Fig. 5 shows that the XRD pattern of BBO and $BaTi(BO_3)_2$ crystals are quite similar and it is thus very difficult to distinguish these two phases. This difficulty is specially enhanced when there is texture.

In previous papers [10,11] some of us have shown that one can distinguish the contributions of β-BBO and $BaTi(BO_3)_2$ by Raman spectroscopy analysis of individual microcrystals on the glass surface. Therefore, before attempting to interpret the X-ray diffraction patterns of the $x_1 = 15\%$ sample presented on Fig. 4, we made a micro-Raman spectroscopic analysis of the structure of the microcrystals present on the surface of this glass in the early stage of crystallization (8 h), and after a long period of heat treatment (32 h). Fig. 6a and b show micrographs of surface crystallized $x_1 = 15\%$ samples after 8 and 32 h of heat treatment, respectively. According to Fig. 6a, only one type of crystal morphology is visible on the surface of a glass sample heat-treated for 8 h. The geometry of these microcrystals is quite similar to that observed by Ding et al. in their $15TiO_2$–$40BaO$–$45B_2O_3$ glass [5]. On the other hand, Fig. 6b shows microcrystals with a different morphology in the sample heat-treated during 32 h. These microcrystals apparently begin to grow underneath (or between the arms of) the previously nucleated microcrystals depicted in Fig. 6a.

To obtain the Raman spectrum of each microcrystal and of the glassy phase in both samples, the laser beam was positioned on the microcrystals and on the glassy phase using an objective lens of 100× which provided a spatial resolution of about 1 μm.

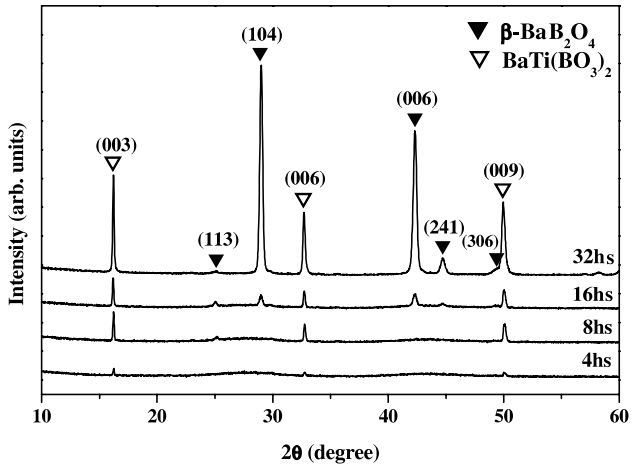

Fig. 4. XRD patterns of a surface crystallized bulk sample with $x_1 = 15\%$, heat-treated for periods varying between 4 h and 32 h. The attribution of the peaks is based on the order of appearance of crystal phases indicated by micro-Raman studies.

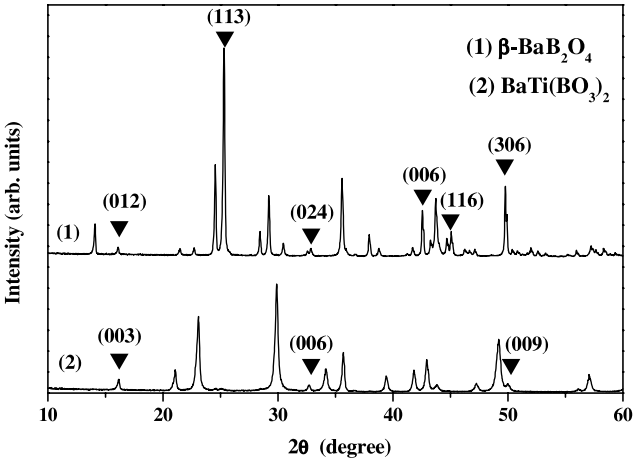

Fig. 5. Comparison between the XRD patterns of β-BaB_2O_4 and $BaTi(BO_3)_2$ crystalline phases used as standards.

Fig. 7 shows the Raman spectra obtained with the laser beam focusing directly upon the microcrystals on the surface of the $x_1 = 15\%$ sample heat-treated for 8 h, identified by the letter B in Fig. 6a. The glassy phase was identified by the letter A. For comparison, the Raman spectrum of $BaTi(BO_3)_2$ reference compound is plotted in the same figure. The Raman spectrum of microcrystal B contains all the Raman lines relating to the $BaTi(BO_3)_2$ crystalline phase. In the same spectrum, a broad Raman line that originated from the glassy phase was also observed around 800 cm^{-1}. This wide Raman band, characteristic of an amorphous phase, indicates that the laser beam passed through the microcrystal and hit the subjacent glassy phase. This assumption is confirmed by the analysis of the Raman spectrum of the glassy phase (spectrum A in Fig. 7), which displays a wide band centered at around 800 cm^{-1}. This result clearly shows that, in the first stage of crystallization and for heating periods of up to 8 h at 620 °C, only $BaTi(BO_3)_2$ crystallizes.

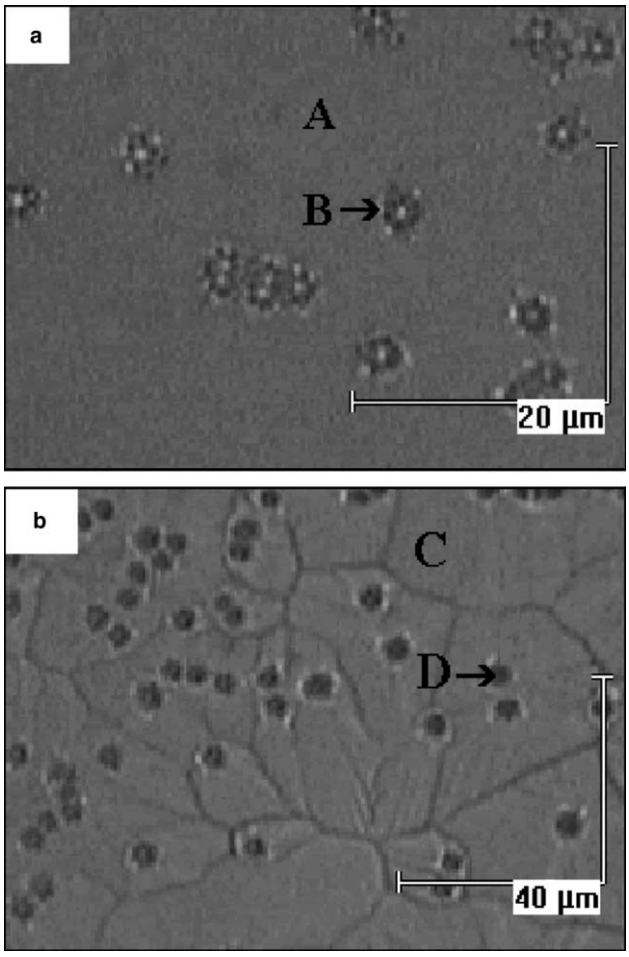

Fig. 6. Optical micrographs of the surface of partially crystallized samples heat-treated at 620 °C for (a) 8 h and (b) 32 h.

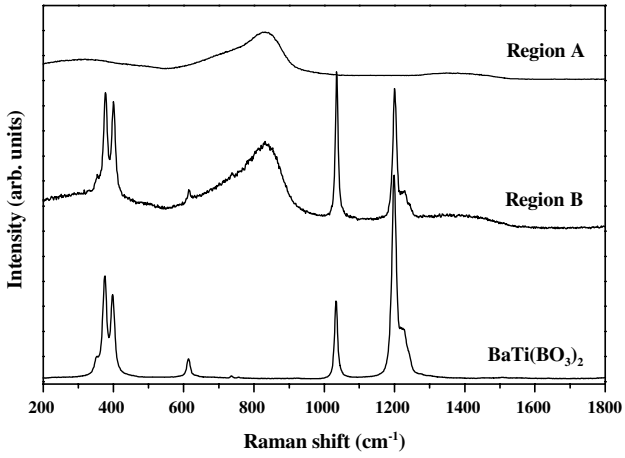

Fig. 7. Raman spectra of the surface regions identified in Fig. 6a: sample heat-treated during 8 h at 620 °C.

Fig. 8 shows the Raman spectra for a laser beam focused on the region called C, and on microcrystals identified as D in Fig. 6b. Our observations indicate that microcrystals C only begin growing after 11 h at this temperature. The microcrystals identified as D in Fig. 6b are the same as those identified as B in Fig. 6a.

For comparison, the Raman spectra of β-BBO and $BaTi(BO_3)_2$ reference compounds are shown in Fig. 8. The Raman spectrum of microcrystal C is quite similar to that of the powdered β-BBO crystals. Although the Raman laser beam was focused only on microcrystal D, beyond the Raman spectrum of the $BaTi(BO_3)_2$ phase, it reveals some lines that were indexed to β-BBO. This means that the laser beam passed through microcrystal D and hit the β-BBO microcrystal that grew just below the former crystalline phase, proving that, in some cases, microcrystals classified as β-BBO grow close to $BaTi(BO_3)_2$ microcrystals after long periods of heat treatment.

In summary, the Raman results for the $x_1 = 15\%$ sample indicated that its devitrification process began with nucleation and growth of $BaTi(BO_3)_2$ microcrystals and that, in the second step, after approximately 11 h at heat treatment at 620 °C, β-BBO microcrystals nucleate and start to grow underneath (or between the arms of) the $BaTi(BO_3)_2$ microcrystals.

Having analyzed the Raman results, the X-ray patterns of the $x_1 = 15\%$ sample shown in Fig. 4 were indexed. The three diffraction peaks observed when the glass was heat-treated for 8 h refer to the (003), (006) and (009) diffraction planes of $BaTi(BO_3)_2$. As the period of heat treatment passed beyond the 11 h mark, other diffraction peaks: (113), (104), (006), (241) and (306) belonging to the β-BBO phase appeared. Thus, long heat treatments led to the appearance of two crystalline phases on the surface of $x_1 = 15\%$ crystallized samples.

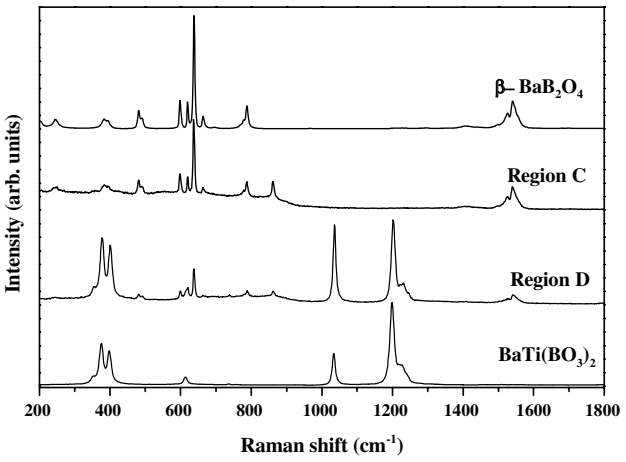

Fig. 8. Raman spectra of the surface regions identified in Fig. 6b: sample heat-treated during 32 h at 620 °C.

3.2. Crystal growth kinetics of $BaTi(BO_3)_2$ on the $x_1 = 15\%$ glass

As we discussed earlier, the $x_1 = 15\%$ sample presented two crystallization stages, the first consisting of the crystallization of $BaTi(BO_3)_2$ and the second, the crystallization of β-BBO. Because $BaTi(BO_3)_2$ crystals act as nucleation sites for β-BBO crystals, we will analyze the crystal growth kinetics of $BaTi(BO_3)_2$. Although the $x_1 = 4\%$ and $x_1 = 8\%$ presented only β-BBO phase after crystallization, the crystal growth kinetics in these samples were not studied because the crystal growth velocities were too high at 620 °C.

Fig. 9(a)–(c) show the time dependence of the average number of crystals per unit area, N_s, maximum radius of crystals, $R(t)$, and fractional area crystallized, respectively. The mean value of N_s was approximately 2×10^{-3} μm^{-2} and did not depend on the heat treatment time up to 10 h at 620 °C. The order of magnitude of N_s is in good agreement with results found in the literature for samples with mechanically polished surfaces [23,24].

We can make an *approximate* analysis of the crystallization kinetics using the Avrami model [19] for heterogeneous nucleation. The surface crystallized fraction (α) is thus given by the following equation:

$$\alpha(t) = 1 - \exp(-\pi N_s R(t)^2) \quad (1)$$

where N_s is the average number of crystals per unit area, and R is the crystal radius. If the growth rate, U, is time-independent, the crystal radius can be related to the heat treatment time, t, by the simple relation [25]:

$$R(t) = Ut \quad (2)$$

Therefore, the fractional crystallized area can be computed by the combination of the previous equations:

$$\alpha(t) = 1 - \exp(-\pi N_s U^2 t^2) \quad (3)$$

and can be compared with experimental values.

The evolution of the fractional crystallized area shown in Fig. 9(c) is reasonably well described by Eq. (3), based on the experimental values of N_s and U ($N_s = 2 \times 10^{-3}$ μm^{-2} and $U = 0.21$ μm/h). According to Fig. 9(c), approximately 2% of the glass surface of the $x_1 = 15\%$ sample was covered with $BaTi(BO_3)_2$ crystals when the sample was heat-treated at 620 °C for 10 h. Crystallization of the β-BBO phase started thereafter.

3.3. Second-harmonic generation (SHG) of surface crystallized glassy samples

The dependence of the intensity of second-harmonic generation on the angle of incidence, that is, the Maker fringe pattern, is shown for three surface crystallized samples in Fig. 10(a)–(c). These patterns were measured under the condition of p-polarized, which means that

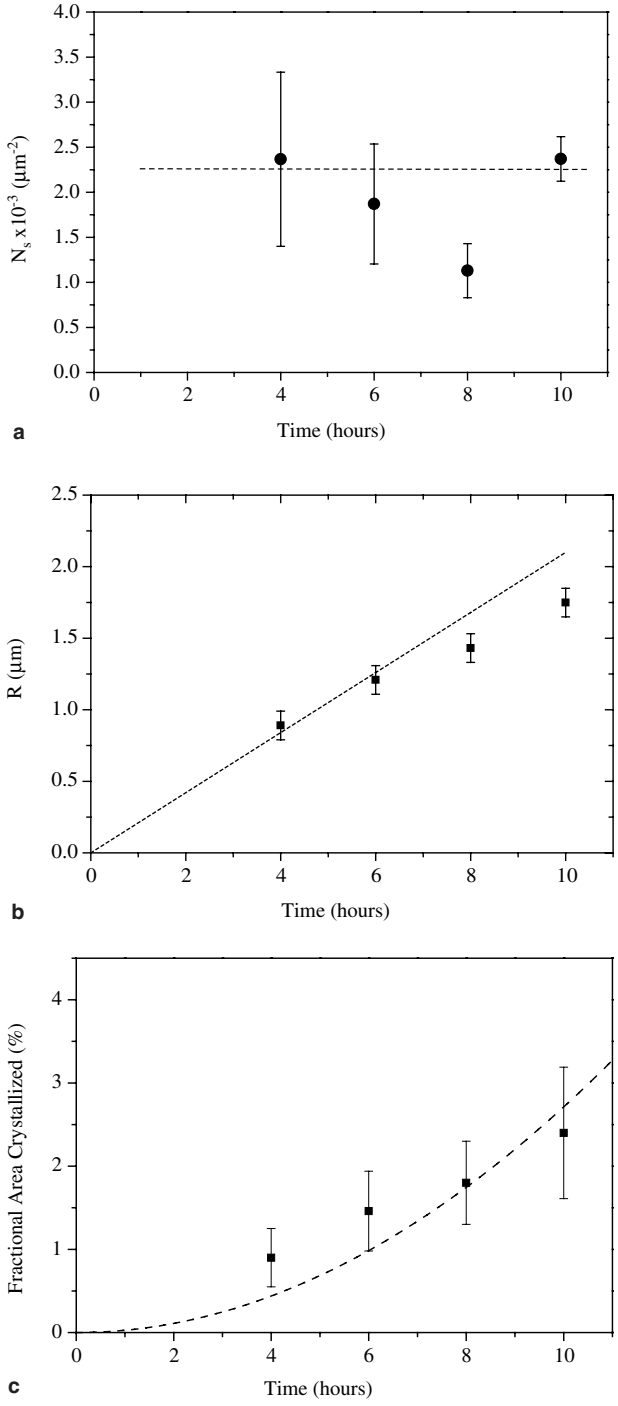

Fig. 9. Time dependence of (a) the average number of crystals per unit area, N_s; (b) maximum crystal radius, R. The straight line just indicates that the crystal growth rate decreases with time, (c) fractional area crystallized, α. The dashed horizontal line on (a) illustrates that there is no increase of N_s with time. The experimental values shown in (b) and (c) were used to produce the calculated curve from Eq. (3) (dotted line), where $N_s = 2 \times 10^{-3}$ μm^{-2} and $U = 0.21$ μm/h.

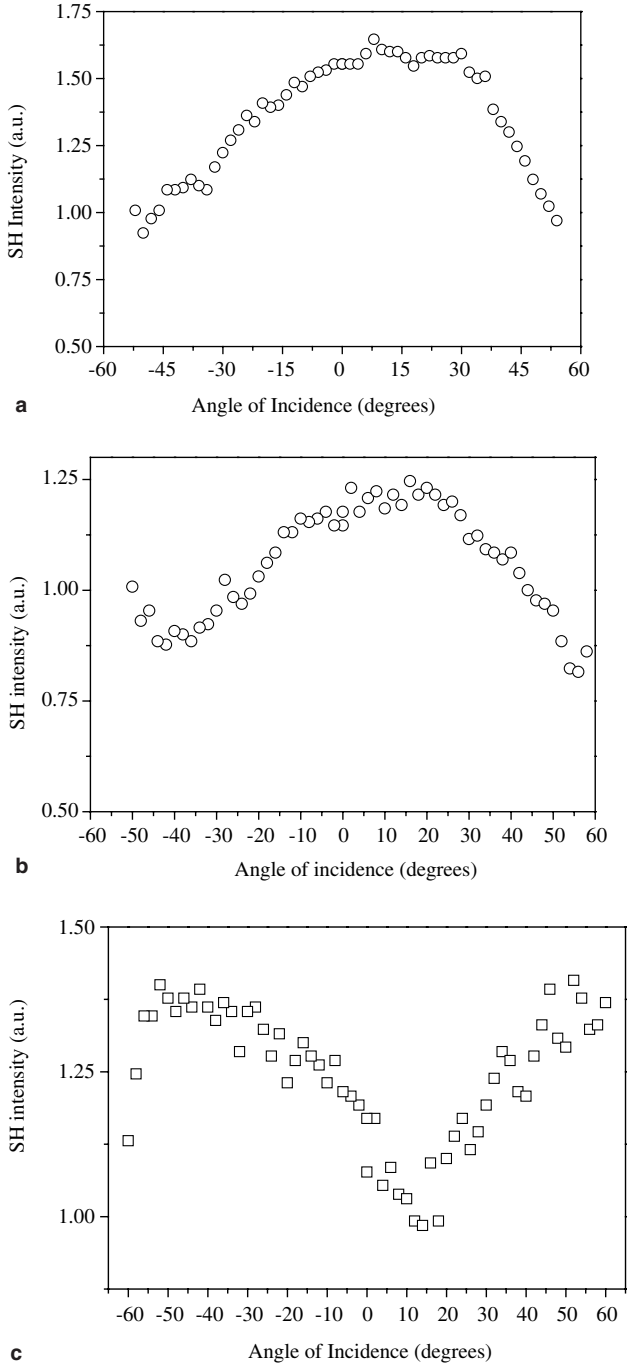

Fig. 10. Variation of second-harmonic intensity with the angle of incidence, i.e., Maker fringe pattern for glasses with (a) $x_1 = 4\%$ TiO_2, (b) $x_1 = 8\%$ TiO_2 and $x_3 = 15\%$ TiO_2. The fundamental and second-harmonic waves were p-polarized.

the plane polarization was parallel to the incident plane for both fundamental and second-harmonic waves. The second-harmonic intensities of the three samples were quite similar. However, the second-harmonic generation in the $x_1 = 15\%$ glass was distinct from those in the $x_1 = 4\%$ and $x_1 = 8\%$ glasses. Whereas these latter two samples presented a maximum intensity around 10°, the $x_1 = 15\%$ sample presented a minimum of the second-harmonic intensity. According to the literature, this difference can be attributed to some structural changes imposed on the origin of the second-harmonic

generation, namely the β-BBO crystals, as the amount of titanium increases [26].

To compare the efficiency of second-harmonic generation of these three samples, we should compare the effective second-order non-linear optical coefficient, d_{eff} [27,28]. According to the work of Lu et al. [27], the SH intensity generated by a fundamental light with intensity $I(\omega)$ is given by

$$I(2\omega) \propto [l_s^2 I^2(\omega) d_{eff}^2 / n^2(\omega) n(2\omega)] \times [\sin^2(\pi l_s/2l_c)/(\pi l_s/2l_c)^2] \quad (4)$$

where l_s is the thickness of the crystallized layer, d_{eff} is the measured effective second-order non-linear optical coefficient, $n(\omega)$ and $n2(\omega)$ are the indexes of refraction at the frequencies ω and 2ω, respectively, and l_c is the coherence length of the crystallized layer.

Using n of bulk β-BBO [29], we found that the calculated β-BBO coherence length, $l_c = \lambda/[4(n(\omega) - n(2\omega))]$, was much *larger* than the crystallized layer thickness l_s. This yielded $[\sin^2(\pi l_s/2l_c)/(\pi l_s/2l_c)^2] \sim 1$. For the calculation of the SH intensity ratio between crystallized layers and quartz, I_s/I_Q, the factor $[n^2(\omega)n(2\omega)/n_Q^2(\omega)n_Q(2\omega)] \sim 1.25$ (where the subscript "Q" denotes values for quartz). If we also take into account the measured transmission, T, of the crystallized layer/glass, the SH signal in Eq. (4) becomes:

$$I_s/I_Q \sim (l_s/l_{c,Q})^2 T d_{eff}^2/(1.25 d_{11,Q}^2) \quad (5)$$

where $l_{c,Q} \sim 20$ μm is the coherence length of quartz and $d_{11,Q} = 0.34$ pm/V is the d_{11} coefficient of quartz [30]. The transmission loss is mainly due to light scattering on the surface of the crystallized layer. This yields:

$$d_{eff} \sim (l_{c,Q}/l_s)[(1.25/T)(I_s/I_Q)]^{1/2} d_{11,Q} \quad (6)$$

The maximum value of d_{eff} in this geometry was calculated using Eq. (6). Table 4 presents the values of d_{eff} for the three samples. Also included is information on the thickness of the crystallized layers, the transmission at 532 and 1064 nm and the degree of orientation for the most important crystallographic planes obtained from the XRD patterns shown in Figs. 1, 3 and 8. According to the data of Table 4, the second-harmonic coefficients are comparable to that of single crystal Y-quartz and, for the sample containing 15% TiO_2, d_{eff} to approximately 50% of the value for single crystalline β-BBO, which is 2.3 pm/V [29].

Table 4
Thickness of the crystallized layer (1 s), transmittance (T) at 532 and 1064 nm, degree of orientation for the most important crystallographic planes and d_{eff} for the three samples

Sample	l_s (μm)	T (%)		f (%)			d_{eff} (pm/V)
		532 nm	1064 nm	(113)	(104)	(006)	
$X_1 = 4\%$	34	34.5	36.8	1	79	10	0.4
$X_1 = 8\%$	75	28.4	31.7	46	21	4	0.2
$X_1 = 15\%$	10	39.2	65.3	10	22	28	1.1

4. Discussion

According to the DSC results, increasing the molar concentration of TiO_2 in the studied glasses reduces their tendency to devitrify. The analysis of the X-ray diffraction patterns confirmed this tendency: the first diffraction peaks of the $x_1 = 4\%$ glass appeared after 1 h of heat treatment at 620 °C, while the first diffraction peaks of the $x_1 = 8\%$ and $x_1 = 15\%$ glasses were observed after 2 and 4 h of heating, respectively.

The surface crystallized samples with 4% and 8% TiO_2 contained only β-BBO crystals even after long heat treatments. In contrast, the surface of partially crystallized glasses containing 15% TiO_2 showed crystallization of $BaTi(BO_3)_2$ for samples heat-treated up to 10 h. Heat-treating this glass for longer periods led to crystallization of a second crystalline phase, β-BBO. As the heat treatment time was extended, the β-BBO phase became the predominant phase. These results show that one can obtain surface crystallized samples containing only the β-BBO phase in glasses containing up to 8% TiO_2.

Spontaneous preferred orientation (texture) was observed in the three surface crystallized glasses, possibly due to the special arrangement of borate molecules in the β-BBO and $BaTi(BO_3)_2$ crystalline structures. It is well-known that the structure of the β-BBO and $BaTi(BO_3)_2$ crystals consist of layers of Ba^{2+} ions and anionic $(B_3O_6)^{3-}$ rings arranged perpendicularly to the c-axis [30]. According to Refs. [31,32], in the case of thin films, the $(B_3O_6)^{3-}$ rings can adjust themselves to lie parallel with the substrate surface provided they possess sufficient kinetic energy. However, the interaction between $(B_3O_6)^{3-}$ rings and Ba^{2+} ions is considered to be strongest in the [104] direction [33]. Therefore, the (104) plane normally also develops easily during crystallization and its X-ray diffraction intensity depends on the glass composition (see Figs. 2, 3 and 8).

Our results show that it is possible to obtain textured surface crystallized samples without introducing foreign particles on the glass surface.

With regard to the $x_1 = 15\%$ glass, our work clearly demonstrated that it was not possible to separate the contribution of the $BaTi(BO_3)_2$ and β-BBO crystalline phases based solely on XRD experiments. We have shown that micro-Raman spectroscopy is an adequate tool to differentiate these two crystalline phases. The similarity between the X-ray diffraction patterns of these two crystalline phases was probably the reason why Ding et al. ascribed the X-ray patterns only to the β-BBO phase [4].

The overall crystallization kinetics of $BaTi(BO_3)_2$ on the surface of the $x_1 = 15\%$ glass showed that this phase

covers approximately 2% of the glass surface when the sample is heat-treated at 620 °C for 10 h, and that crystals of this phase may act as nucleation sites for the β-BBO phase.

Second-harmonic generation tests indicated that the best results were obtained for the $x_1 = 15\%$ glass. The most important difference between the three glasses was the degree of texture of some crystallographic planes. As can be observed in Table 4, the $x_1 = 15\%$ sample displayed the best orientation in the (006) direction. These results agree with those of other authors who measured the second-harmonic efficiency of β-BBO thin films presenting [006] orientation, which exhibit the highest second-harmonic generation [32–34].

5. Conclusions

Increasing the molar concentration of TiO_2 reduces the devitrification tendency of the glasses studied here. Partially crystallized samples containing 4% and 8% TiO_2 yielded only the β-BBO phase, even with long periods of heat treatment. On the other hand, only $BaTi(BO_3)_2$ crystallized on the surface of samples containing 15% TiO_2 heat-treated up to 8 h. However, as the period of heat treatment increased, β-BBO became the predominant phase, indicating that surface crystallized glasses containing mostly or only β-BBO can be obtained. Spontaneous preferred orientation occurred in the three glasses and may have been due to the special arrangement of the borate units in the β-BBO and $BaTi(BO_3)_2$ crystalline structures. Micro-Raman spectroscopy proved an adequate tool to differentiate these two crystalline phases, which displayed very similar diffraction patterns.

Second-harmonic generation was examined in three surface crystallized samples. The $x_1 = 15\%$ glass presented the highest value of the SHG coefficient, which reached approximately 50% of the value observed for β-BBO single crystal. This behavior was attributed to the preferred orientation of β-BBO crystals in the [006] direction on the glass surface.

Acknowledgement

We are indebted to FAPESP, PRONEX, CAPES and CNPq (Brazil) for their financial support.

References

[1] A. Bhargava, R.L. Snyder, R.A. Condrate, Mater. Res. Bull. 22 (1987) 1603.
[2] A. Bhargava, J.E. Shelby, R.L. Snyder, J. Non-Cryst. Solids 102 (1988) 136.
[3] K. Kusumoto, T. Sekiya, Y. Murase, Mater. Res. Bull. 28 (1993) 461.
[4] Y. Ding, A. Osaka, Y. Miura, J. Am. Ceram. Soc. 77 (1994) 749.
[5] P. Pernice, S. Esposito, A. Aronne, Phys. Chem. Glasses 39 (1998) 222.
[6] A. Aronne, S. Esposito, P. Pernice, Phys. Chem. Glasses 40 (1999) 63.
[7] C.T. Chen, B. Wu, A. Jiang, G. You, Sci. Sinica B28 (1985) 235.
[8] V.N. Sigaev, S. Yu Stefanovich, B. Champagnon, I. Gregora, P. Pernice, A. Aronne, R. LeParc, P.D. Sarkisov, C. Dewhurst, J. Non-Cryst. Solids 306 (2002) 238.
[9] Y. Ding, Y. Miura, S. Nakaoka, T. Nanba, J. Non-Cryst. Solids 259 (1999) 132.
[10] A.F. Maciente, V.R. Mastelaro, A.L. Martinez, A.C. Hernandes, C.A.C. Feitosa, J. Non-Cryst. Solids 306 (2002) 309.
[11] A.F. Maciente, V.R. Mastelaro, A.L. Martinez, A.C. Hernandes, C.A.C. Feitosa, J. Non-Cryst. Solids 318 (2003) 331.
[12] T.J. Headley, R.E. Loehman, J. Am. Ceram. Soc. 67 (1984) 620.
[13] C.L. Liu, S. Komarneni, R. Roy, J. Am. Ceram. Soc. 75 (1992) 2665.
[14] U. Selvaraj, C.L. Liu, S. Komarneni, J. Am. Ceram. Soc. 74 (1991) 1387.
[15] K.H. Ashbee, J. Mater. Sci. 10 (1975) 911.
[16] D.I.H. Atkinson, P.W. McMillan, J. Mater. Sci. 12 (1997) 443.
[17] B.R. Durschang, G. Carl, C. Rüssel, K. Marchetti, E. Roeder, Glastech. Ber. Glass. Sci. Technol. 67 (1994) 171.
[18] K. Engel, G.H. Frischat, Texture Microstruct. 24 (1995) 155.
[19] N. Diaz-Mora, E.D. Zanotto, R. Hergt, R. Müller, J. Non-Cryst. Solids 273 (2000) 81.
[20] G.J. Gardopee, R.E. Newnham, A.S. Bhalla, Ferroelectrics 155 (1981) 33.
[21] L.J.Q. Maia, C.A.C. Feitosa, F.S. De Vicente, V.R. Mastelaro, M. Siu Li, A.C. Hernandes, J. Am. Soc. Vac. Thin Films A22 (5) (2004) 1.
[22] P.D. Maker, R.W. Terhune, M. Nisenoff, C.M. Savage, Phys. Rev. Lett. 8 (1962) 21.
[23] R. Muller, E.D. Zanotto, V.M. Fokin, J. Non-Cryst. Solids 274 (2000) 208.
[24] E.D. Zanotto, V.M. Fokin, Philos. Trans. R. Soc. London A 361 (2003) 591.
[25] E.D. Zanotto, J. Non-Cryst. Solids 130 (1991) 217.
[26] A. Narazaki, K. Tanaka, K. Hirao, J. Mater. Res. 14 (9) (1999) 3640.
[27] H.A. Lu, L.A. Wills, B.W. Wessels, W.P. Lin, T.G. Zhang, G.K. Wong, D.A. Neumayer, T.J. Marks, Appl. Phys. Lett. 62 (1993) 1314.
[28] Y.R. Shen, The Principles of Nonlinear Optics, Wiley, New York, 1984, p. 72.
[29] D.N. Nikogosyan, Properties of Optical and Laser-Related Materials: A Handbook, John Wiley & Sons, England, 1997, p. 78.
[30] S. SinghHandbook of Laser Science and Technology, Part 1, vol. III, Chemical Rubber, Boca Raton, FL, 1986, p. 75.
[31] D. Eimer, L. Davis, S. Velsko, E.K. Graham, A. Zalkin, J. Appl. Phys. 62 (1987) 1968.
[32] R.F. Xiao, L.C. Ng, P. Yu, G.K.L. Wong, Appl. Phys. Lett. 67 (1995) 305.
[33] H.B. Liao, R.F. Xiao, P. Lu, G.K.L. Wong, J.Q. Zheng, J. Vac. Sci. Technol. A 14 (1996) 2651.
[34] D.B. Studebaker, G.T. Stauf, T.H. Baum, T.J. Marks, H. Zhou, G.K. Wong, Appl. Phys. Lett. 70 (5) (1997) 565.